第42卷第3期 红外与毫米波学报 Vol. 42, No. 3
2023年6月 J. Infrared Millim. Waves June, 2023

文章编号:1001-9014(2023)03-0339-06 DOI:10. 11972/j. issn. 1001-9014. 2023. 03. 007

High power added efficiency AlGaN/GaN MIS-HEMTs for wide band application

CHEN Xiao-Juan[1,2*], ZHANG Shen[2], ZHANG Yi-Chuan[2], LI Yan-Kui[2], GAO Run-Hua[2], LIU Xin-Yu[2], WEI Ke[2*]

(1. Xidian University, Xi'an 710071, China;
2. Institute of Microelectronics, Chinese Academy of Sciences, Beijing 100029, China)

Abstract: In this study, we report a new design of GaN metal insulation semiconductor - high electron mobility transistor (MIS-HEMT) device with a 5 nm high-quality SiN_X dielectric layer deposited between gate and AlGaN barrier layer, to reduce the gate reverse leakage and improve power added efficiency (PAE). Superior characteristics of the device are proved in DC, small signal and large signal tests, showing the improved device owing a high-quality interface, a wide-control-range gate, the capability to control current collapse and the ability to maintain high PAE when serving at frequency higher than 5 GHz. Serving at 5 GHz with V_{DS} = 10 V, the device showed an output power of 1. 4 W/mm, with PAE of 74. 4%; when V_{DS} rises to 30 V, output power increases to 5. 9 W/mm with PAE remaining at 63. 2%; a high PAE (50. 4%) remained even when the test frequency increased 30 GHz while keeping the same output power. Additionally, the high-quality gate dielectric layer allows the device to withstand a wide gate voltage swing: the gate current remained 10^{-4} A/mm even gain compressed to 6 dB. The results demonstrate the improvement of the SiN_x on MIS-HEMT device, which provides device-level guarantee for the power application of the system and the design of broadband circuits.

Key words: metal-insulator-semiconductor High Electron Mobility Transistors (MIS-HEMTs), power added efficiency (PAE), broadband, compressed gain, gate voltage swing

应用于宽带的AlGaN/GaN MIS-HEMT高效率器件

陈晓娟[1,2*], 张 昇[2], 张一川[2], 李艳奎[2], 高润华[2], 刘新宇[2], 魏 珂[2*]

(1. 西安电子科技大学,陕西 西安 710071;
2. 中国科学院微电子研究所,北京 100029)

摘要:本文采用等离子体增强原子层沉积(PEALD)生长的SiN_x栅介质制备了宽带应用的AlGaN/GaN金属绝缘体半导体高电子迁移率晶体管(MIS-HEMTs),并在直流、小信号及大信号测试中评估了该介质层对器件性能的提升。测试结果表明改进器件具有高质量界面、宽栅极控制范围、良好的电流崩塌控制等优势,并确认了其在超过5 GHz下工作时仍能保持较高的功率附加效率(PAE)。在5 GHz连续波模式下,漏极电压V_{DS}= 10 V时,MIS HEMT输出功率密度为1.4 W/mm,PAE可达到74.7%;V_{DS}增加到30 V时,功率密度提升到5.9 W/mm,PAE可保持在63.2%的水平;测试频率增加30 GHz,在相同的输出功率水平下,器件的PAE达到50.4%。同时,高质量栅极介电层还可允许器件承受高的栅极电压摆动:在功率增益压缩6 dB时,栅极电流保持在10^{-4} A/mm。上述结果证实了该SiN_x栅介质对器件性能的提升,使其满足宽带应用的高效率、高功率和可靠性要求,为系统和电路的宽带设计提供器件级的保障。

关 键 词:MIS-HEMTs;SiN_x栅介质;功率附加效率;栅压摆幅;宽带

中图分类号:O48 **文献标识码**:A

Received date: 2022-09-29, **revised date**: 2023-02-20 **收稿日期**:2022-09-29,**修回日期**:2023-02-20

Foundation items: Supported by the National Natural Science Foundation of China (61822407, 62074161, 62004213); the National Key Research and Development Program of China under (2018YFE0125700)

Biography: Chen Xiaojuan (1979-), female, ChongQing, master. Research area involves Compound Semiconductor materials and devices. E-mail: chenxiaojuan@ime. ac. cn.

[*] **Corresponding authors**: E-mail: chenxiaojuan@ime. ac. cn, weike@ime. ac. cn

Introduction

The wireless communication technology has entered the 5G era, while the corresponding system needs to support higher throughput and faster information transmission. Meanwhile, the advantages of 5G technology, such as high peak-to-average power ratio of signal, wide bandwidth, and small size of hardware system, has raised new demands to the radio frequency system. The broadband power amplifier is a critical module in the system, and power added efficiency (PAE) and bandwidth performance have been considered to be key parameters that reveals its efficiency[1]. Many approaches have been proposed to improve the efficiency in last decade[2]-[6]. Lu Y. et al. developed achieved AlGaN/GaN HEMT by the Recess-arrayed Ohmic Contact technology [7], with the PAE of 71.6% at 5 GHz, which further attained 85.2% after the third harmonic tuning. Wienecke [8] et al. developed an AlGaN/GaN MIS-HEMT structure using N-Polar GaN material with SiC as substrate, and its PAE attained 54.9%, 52.5%, and 26.9% with continuous output power of 8 W/mm at 10 GHz, 30 GHz, and 94 GHz, respectively.

For the broadband circuit, when the device works in narrow band, both efficiency and bandwidth can be taken into account; however, when the device works at high frequency and reaches the power index, the low-frequency area is often in a saturated state, where the harmonic component increases, resulting in the increase of gate current, hence the biased gate voltage leading the power decline of the circuit at the low-frequency area. To meet the requirements of broadband work, traditional HEMT devices with Schottky gate metal contacts have been widely used to improve the quality of the gate because the low Schottky forward barrier reduces the reverse leakage of the gate, which is one of the current leakage channels that aggravates the device loss and reduces the effective voltage loaded on the gate. However, when the device works in a saturated state, the gate voltage exceeding the Schottky barrier will lead to a rapid increase in the gate current, and even cause the device to fail.

In this study, a SiN_x gate dielectric was introduced to compose an AlGaN/AlN/GaN MIS-HEMT structure, which is supposed to reduce the gate reverse leakage and improve PAE. Effects of the dielectric layer on swing of the gate forward working voltage, interfacial status, and frequency characteristics of devices were investigated, thus its feasibility of applying in broadband circuits was demonstrated.

1 Experiments

1.1 Material structure

The AlGaN/GaN epitaxial material structure used in this study is shown in Fig. 1(a) and described from bottom to top as the following. A SiC substrate with thickness of 280 nm was used for heat dissipation. An18-nm AlN nucleation layer was used to release the lattice stress generated by the lattice and thermal adaptation, and to reduce the background carrier concentration. Then, a high resistance GaN buffer layer with a thickness of 2 μm was deposited to reduce device leakage and avoid efficiency loss caused by device leakage in high fields. Another AlN layer with a thickness of 1 nm was deposited to form a deeper and narrower quantum well, which is beneficial to improve the channel electron density. With the AlN layer, the following undoped AlGaN barrier layer, with its thickness of 14 nm, were prevented from penetration of two-dimensional electron gas, so that the disordered scattering of carriers and the channel electron mobility could be improved [9]. A SiN_x cap layer was then deposited to generate compressive stress on the barrier layer and negative charge caused by polarization, strengthening the positive charge on the upper surface of the AlGaN barrier layer, so as to shield the influence of AlGaN surface state on channel electrons, and help to suppress the current collapse effect [10]. The square resistance of the final material is 310 Ω/square, and the mobility is more than 2 000 cm^2/Vs.

1.2 Device structure

The structure of the device is shown in Fig. 1(a-c). The source-drain distance (L_{SD}), gate-drain distance (L_{GD}), gate length, and gate cap of the MIS-HEMT are 2.4 μm, 1.15 μm, 0.25 μm, and 0.7 μm, respectively. The recessed-gate width and depth are 0.8 μm and 6 nm, respectively. The three-dimensional shape of the gate adopts a U-shaped gate structure [11], which is helpful to reduce the electric field between the gate and drain and to improve the breakdown voltage, thereby the output power density and power additional efficiency of the device are improved.

1.3 Device fabrication

The device is fabricated by a 0.25 μm gate length process: started by W metal as the marker, then source and drain recess was etched, Ti/Al/Ni/Au layers as the ohmic contact metal stack were deposited. Finally, the structure was rapid thermal annealed at 800 ℃ for 30 s in N_2 ambient, yielding a contact resistance of 0.3 Ω·mm, and device isolation was formed utilizing multiple-energy nitrogen ion implantation.

In order to improve the gate control ability and reduce the distance from the gate to the channel, a low-damage atomic layer etching method was used to obtain the recessed-gate [12]. The 5 nm SiN_X layer was deposited by PEALD method and was annealed at 650 ℃ for 4 minutes in O_2 atmosphere [13]. T-shaped gate was subsequently accomplished by electron beam lithography (EBL) of UVIII/Al/PMMA resist stack. Width of the T-gate foot and head are 0.25 μm and 0.7 μm respectively. Ni/Au layers were deposited as gate metal, then the device was passivated with 200 nm SiN_x grown by PECVD method. Finally, the electrodes were electroplated to 3 μm. The finished device is shown in Fig. 1(b), and Fig. 1(c) shows a TEM picture of the gate area.

2 Results and discussions

2.1 C−V measurement

The capacitance-voltage (C-V) measurement is employed to estimate interface trap density. The frequency

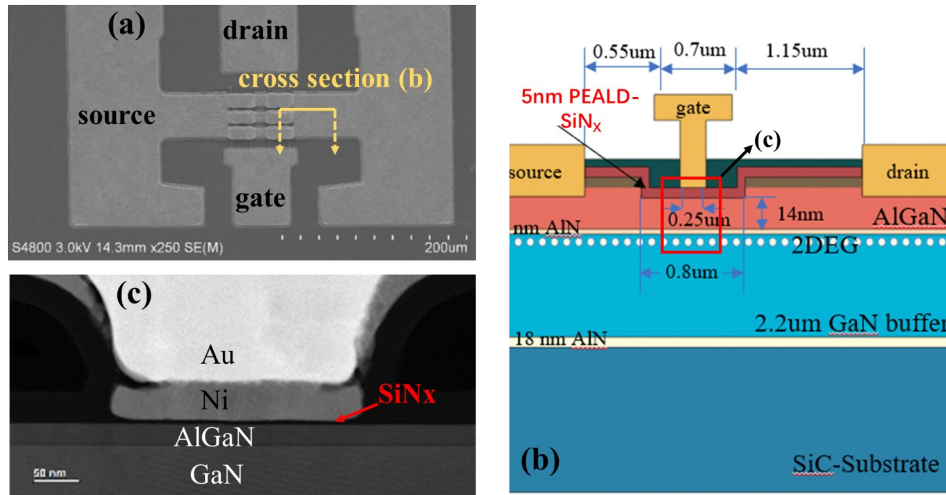

Fig. 1　Diagram of the AlGaN/GaN MIS-HEMT (a) SEM of 4×50μm device, (b) the schematic of epitaxial structure, (c) TEM of 0. 25-μm T-gate
图1　AlGaN/GaN MIS-HEMT (a) 4×50 um器件SEM图片,(b)材料与器件结构示意图,(c)栅处的TEM图片

dispersion of the second slope in the C-V curves [14] was analyzed with F_M varying from 10 kHz to 500 kHz at R. T., as shown in Fig. 2. The slight dispersion (ΔV = 0. 24 V) was used to calculate the interface trap density D_{it}, which falls below 7. 1×10^{12} $cm^{-2}eV^{-1}$ with E_C decrease from -0. 33 eV to − 0. 45 eV, as shown in the inserted image; this low D_{it} indicates high interface quality of the MIS-HEMT.

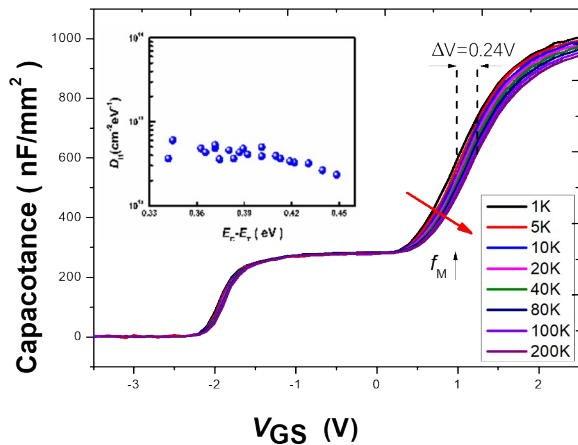

Fig. 2　f-dependent C-V characteristics of AlGaN/GaN MIS-HEMTs with f_m varying from 1 KHz to 200 KHz, inserting D_{it}-E_T mapping in AlGaN/GaN MIS-HEMTs
图2　AlN/GaN MIS-HEMTs不同频率下的CV测试图,插入图为AlGaN/GaN MIS-HEMTs多频下计算的Dit-ET关系图

2. 2　DC measurement

The DC current-voltage characteristics of the AlGaN/GaN MIS-HEMTs were measured by keithly 4 200, and the output characteristics of the device are shown in Fig. 3(a). When V_{GS} = 2 V, the maximum output density was 1. 2 A/mm, and the knee voltage (V_{KNEE}) was 2. 9 V, which reveals a good ohmic contact that promise low energy consumption and high device efficiency.

Transfer characteristics were measured at V_{DS}= -6 V with the V_{GS} ranging from -6 V to 2 V. A maximum G_M of 435 ms/mm was attained when V_{GS} = -0. 2 V, and threshold voltage (V_{TH}) was measured to be -1. 6 V, while V_{GS} = 2 V, I_{DS} = 1. 2 A/mm, as shown in Fig. 3(b).

The validity of the MIS-HEMT is generally reflected by gate performance. As shown in Fig. 3 (c), with V_{GS} sweeping from -30 V to 6 V, the leakage current merely reached 1×10^{-8} A/mm when the reverse V_{GS} = -30 V, which is 2~3 orders of magnitude lower than that of the normal Schottky gate structure. Meanwhile, when the positive gate voltage V_{GS} = 6 V, the forward current reached 3. 59×10^{-6} A/mm, that demonstrated the prior reliability of the improved MIS-HEMT device even under a high V_{GS}. Meanwhile, the Schottky barrier is maintaining only 1. 6 V ~ 1. 8 V [12]. Therefore, the gate voltage of the MIS-HEMT has a wider control range, which ensures its reliability under condition of saturated power serving.

The breakdown voltage was measured with the V_{GS} fixed at -4, the leak voltage V_{DS} set from 0 V to 150 V, and the breakdown current limited to 10 mA/mm. When V_{DS} varied from 0 V to 53 V under the off-state operation, the current was below 10^{-4} A/mm. However, the leakage rose sharply when V_{DS} reached 105 V, which was the drain-source breakdown voltage of the device.

2. 3　Small-signal measurement

The small signal characteristics of the device were measured by Agilent E8363B Vector Network Analyser, with a test range from 100 MHz to 40 GHz and V_{GS}=-0. 5 V. As shown in Fig. 4, when V_{DS} = 10 V, the current-gain cutoff frequency f_T = 49. 5 GHz, the unit-power-gain frequency f_{max} = 88. 1 GHz. When V_{DS} = 30 V, the f_T = 39. 2 GHz, f_{max} = 100. 9 GHz. The increasing initial gain results in an increase in the corresponding MAG. The f_T and f_{max} under different V_{DS}, as depicted in the inserted diagram, suggests that as V_{DS} grows, f_T drops because the increasing V_{DS} enhances the electric field strength between the gate and drain, hence the deterioration of the elec-

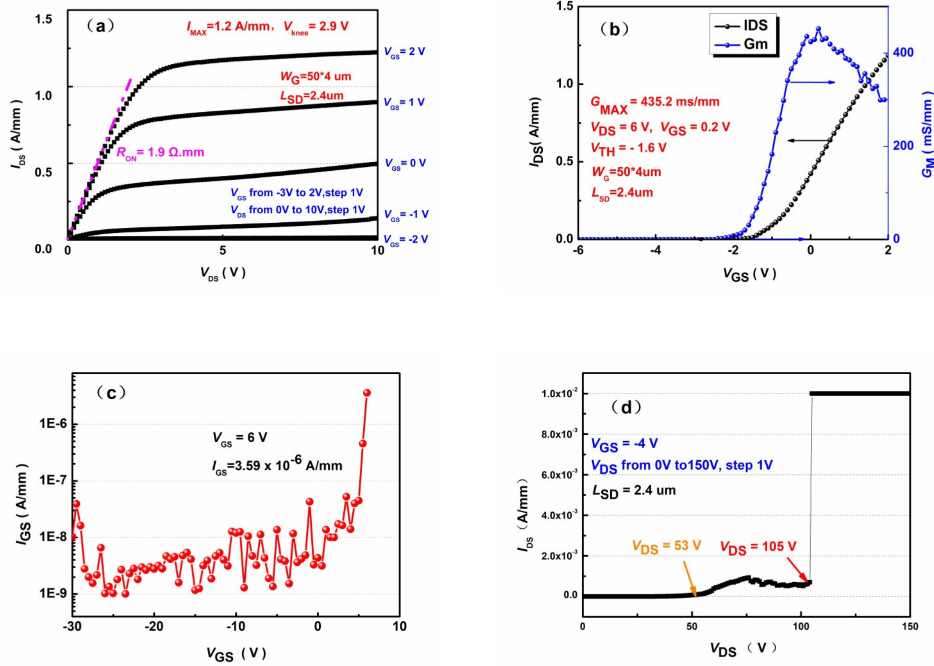

Fig. 3 Measured dc characteristics of AlGaN/GaN MIS-HEMTs (a) I_D versus V_{DS} with V_{GS} varied from -6 V to 2 V, (b) I_D and extrinsic transconductance of MIS-HEMTs with V_{GS} varied from -6 V to 2 V at V_{DS}= 6 V, (c) gate leakage with V_{GS} swept to -30 V, (d) off-state breakdown characteristics at V_{GS}=4 V

图3 AlGaN/GaN MIS-HEMT器件(a)输出电流特性测试图,(b)器件转移特性测试图,(c)栅特性测试图,(d)关态击穿特性测试图

tron saturation velocity. The decrease of trans-conductivity reduces f_T, whereas f_{max}, despite the current decreases, the increase of RF power caused by the higher V_{DS} increases the gain of the device, and the corresponding f_{max}, up to power gain equal to one also increases. As the V_{DS} approaches $V_{BR}/2$, the power reaches its saturation point, the f_{max} also reaches the highest, where V_{DS} = 30 V and f_{max} = 102 GHz, as shown in the insert diagram.

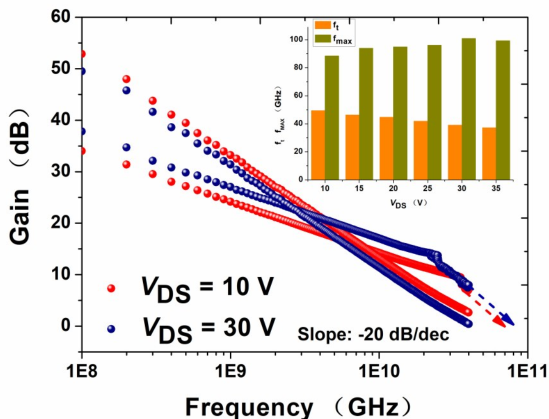

Fig. 4 Small-signal characteristics of the fabricated AlGaN/GaN MIS-HEMTs at V_{DS} = 10 V/30 V, inserting f_T and f_{max} with different V_{DS}

图4 VDS = 10 V/30 V下MIS-HEMTs器件小信号测试图;插入图为频率特性随漏压的变化图

2.4 Pulse measurement

The pulse I-V test, with the pulse cycle time, pulse signal width, and the duty cycle set to 10 μs, 200 ns, and 2%, respectively, was conducted to estimate current collapse of the device. The static offset point was set to (V_{GSQ}, V_{DSQ}) = (0 V, 0 V) and the electrical stress for the gate area was set to (V_{GSQ}, V_{DSQ}) = (-6 V, 0 V), and the results are shown in Fig. 5. The extent of the I_{DS} deterioration with different electrical stress reveals the effect of the traps related to the gate on the frequency dispersion effect, namely the gate-lag. The gate-lag of this device was 1.83% at the knee point voltage position, and it was almost completely restored when V_{DS} = 10 V. When the drain voltage stress increased to (V_{GSQ}, V_{DSQ}) = (-6 V 10 V)/(-6 V, 15 V)/(-6 V 20 V), the drain-lag values were 8.46%, 12.77%, and 17.93% at the V_{KNEE} respectively; the results suggest that the current collapse effect of the device is well controlled.

2.5 Large signal measurement

Based on the Load-Pull test system, a 4×50 μm gate-width device was tested by a continuous wave (CW) signal with a frequency of 5 GHz. Load pull at the input and output impedance points was carried out on all devices for optimal efficiency. Device was biased in class AB at I_{BIAS}=10% I_{MAX}. The device power curve obtained is shown in Fig. 6(a), when V_{GS}= -0.5 V, V_{DS}=10 V, the input impedance point Zsource =43.84 + j95.28, and the output impedance point Zload =147.18 + j76.48, the linear gain of the device was 17.2 dB, the saturated output power was 24.3 dBm (1.4 W/mm), and the PAE

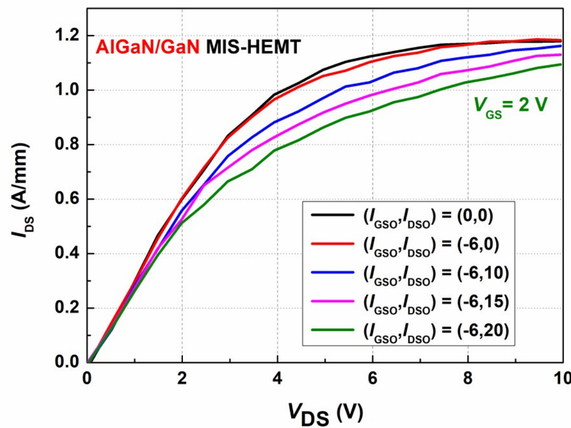

Fig. 5 Pulsed I-V characteristics of output characteristics measured at V_{GS} = 2 V with different static stress
图5 VGS = 2 V下不同静态偏置下饱和输出电流脉冲测试对比

reaches 76.1%. A similar pattern was observed when V_{DS} increased to 30 V, as shown in Fig. 6(b), the linear gain of the device was 20.1 dB, the saturated output power was 30.7 dBm (5.9 W/mm), and the PAE reached 63.2%. Output power and efficiency under wider V_{DS} range was further evaluated, and a comparison diagram is shown in Fig. 6(c), which suggests that the increasing V_{DS} enhanced the output power with only a slight decrease in the efficiency. The above results indicate the excellent efficiency performance of the device at 5 GHz.

Additionally, noted from Fig 6(a) and (b) that the maximum efficiency of the device was obtained at the P_{3dB} compression point. Since the static voltage of the device is V_{GS}= -0.5 V and the V_{PP} is 2 V when P_{IN} = 10 dBm, the voltage on the gate is higher with the increase of P_{IN}. The positive wide swing of the MIS-HEMT device ensures the stability of the gate and the device efficiency continues to increase.

As mentioned, when the device is further compressed, the harmonic component increases and the gate current fluctuates. Fig. 7 shows the gate current recorded by power sweeping in the load-pull test. When P_{IN} = 15 dBm, the power was compressed within 5 dB, and the gate current maintained at 10^{-5} A/mm. When the device is further compressed to 6 dB, the gate current rises to 1.7 mA/mm, and the device still worked normally. The excellent gate characteristics of MIS-HEMTs ensure the power flatness working in full frequency band.

The device was also evaluated by a CW large signal with a frequency of 5, 10 and 30 GHz. Device was biased in class AB at 0.1 A/mm(~10% I_{DS}, max), and V_{DS} was fixed at 30 V. The load reflection coefficient (Γ_{load}) was tuned considerating both efficiency and output power. The output power of all frequency points exceeded 5 W/mm. As shown in Fig. 8, with the frequency of 5, 10, and 30 GHz, the lineal gains are 20.1 dB, 16.9 dB and 10.3 dB, respectively, and the efficiency under high output power are 63.2%, 59.4% and 50.4%, respectively. The results demonstrate the outstanding performance of the device for broadband application.

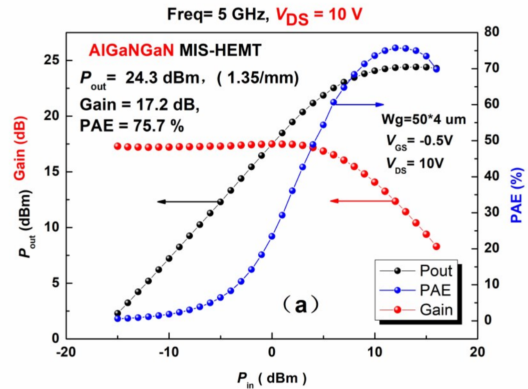

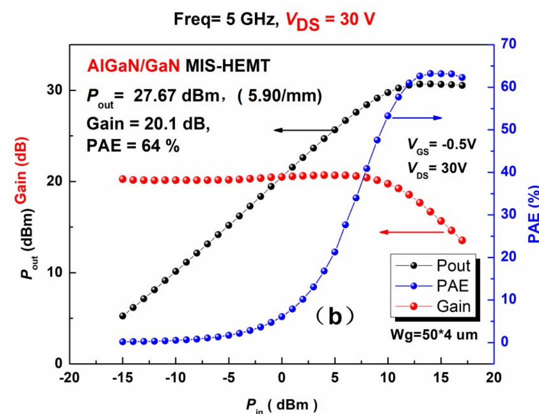

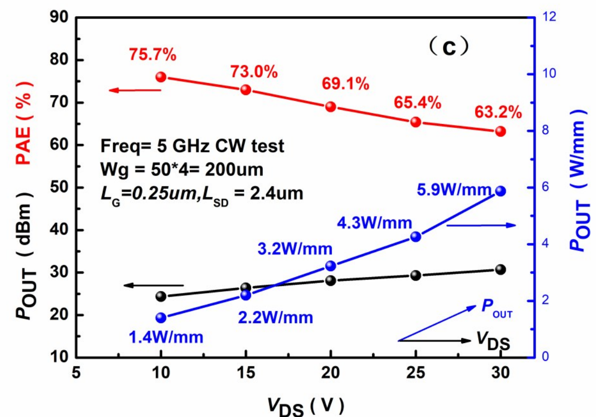

Fig. 6 Large-signal measurements at 5 GHz in CW mode (a) V_{DS} =10 V, AlGaN/GaN MIS-HEMTs measurement, (b) V_{DS}=30 V, AlGaN/GaN HEMTs measurement, (c) with different V_{DS} AlGaN/GaN MIS-HEMTs large-signal performance diagram
图6 5 GHz下大信号连续波测试(a)VDS = 10 V, AlGaN/GaN MIS-HEMTs测试结果,(b)VDS = 30 V, AlGaN/GaN HEMTs测试结果,(c)大信号特性随VDS的变化图

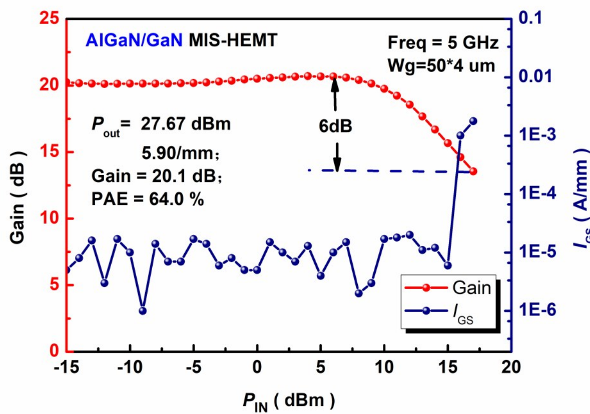

Fig. 7 Graph of I_{GS} and Gain versus Pin
图7 栅电流和增益随Pin的变化图

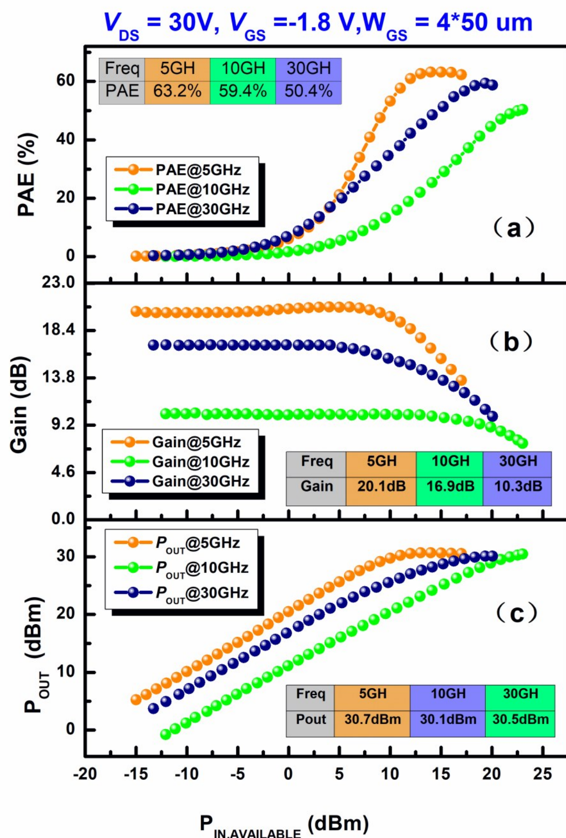

Fig. 8 Large-signal measurements at 5 GHz/10 GHz/30 GHz (a) PAE characteristic, (b) Gain characteristic, (c) Pout characteristic
图8 5 GHz/10 GHz/30 GHz下器件大信号测试图(a)功率附加效率对比图,(b)增益对比图,(c)输出功率对比图

3 Conclusions

In this study, a SiN_x dielectric layer was stacked on the Schottky gate of HEMT to improve the characteristics of the gate project. Performance results in DC, small signal, and large signal tests suggest that the high-quality dielectric layer not only reduced the reverse leakage of the gate, but also increased the positive swing of the gate bias voltage, hence the guarantee for device serving reliably under saturated output power condition. Based on the device design and process conditions in this study, the additional power efficiency reached 75. 6% at C-band when low drain bias voltage V_{DS}=10 V, and 63. 2% when V_{DS}=30 V. Even when the frequency increased to 30 GHz with V_{DS} kept at 30 V, PAE still maintained at 50. 4%. The high efficiency of devices is the prerequisite for the communication system, providing device-level guarantee for stable power system and design of broadband circuit.

References

[1] W. Chen, Lv G., Liu X., *et al*. Doherty PAs for 5G Massive MIMO: Energy-Efficient Integrated DPA MMICs for Sub-6-GHz and mm-Wave 5G Massive MIMO Systems [J]. *IEEE Microwave Magazine*, 2020, **21** (5): 78-93.

[2] ABDULKHALEQ A M, YAHYA M A, PARCHIN N O, *et al*. Mutual Coupling Effect on Three-Way Doherty Amplifier for Green Compact Mobile Communications; proceedings ofthe 14th European Conference on Antennas and Propagation (EuCAP 2020), F, 2020 [C].

[3] SEIDEL A, WAGNER J, EFFINGER F, *et al*. 3.6 GHz Asymmetric Doherty PA MMIC in 250 nm GaN for 5G Applications [M]. Proceedings of the 2020 German Microwave Conference. 2020: 1-4

[4] Weijin Luo, Xiaojuan Chen, *et al*. A C-hand GaN based linear power amplifier with 55.7% *PAE*, solid-state electronics 54 (2010) **457**-460

[5] Wang Feipeng, Yang A. H., Kimball D. F., *et al*. Design of wide-bandwidth envelope-tracking power amplifiers for OFDM applications [J]. *IEEE Transactions on Microwave Theory and Techniques*, 2005, **53** (4): 1244-1255.

[6] T. Torii, Imai S., Maehara H., *et al*. 60% PAE, 30W X-band and 33% PAE, 100W Ku-band PAs utilizing 0.15 μm GaN HEMT technology [C]. 2016 46th European Microwave Conference (EuMC), 2016, 568-571.

[7] Lu Y, Ma X, Yang L, *et al*. High RF Performance AlGaN/GaN HEMT Fabricated by Recess-Arrayed Ohmic Contact Technology [J]. *IEEE Electron Device Letters*, 2018: 1-1.

[8] B. Romanczyk, *et al*., "Demonstration of Constant 8 W/mm Power Density at 10, 30, and 94 GHz in State-of-the-Art Millimeter-Wave N-Polar GaN MISHEMTs," in IEEE Transactions on Electron Devices, vol. **65**, no. 1, pp. 45-50, Jan. 2018, doi: 10.1109/TED.2017.2770087.

[9] Ni Jin-Yu, Hao Yue, Zhang Jin-Cheng, *et al*. Influence of high-temperature AlN interlayer on the electrical properties of AlGaN/GaN heterostructure and HEMTs [J]. ACTA PHYSICA SINICA, 2009 (7): 6. (倪金玉, 郝跃, 张进成, 等. 高温AlN插入层对AlGaN/GaN异质结材料和HEMTs器件电学特性的影响[J]. **物理学报**), 2009(7): 6.

[10] Zhao Miao, Liu Xinyu, *et al*. Effect of GaN Cap on Schottky Properties of AlGaN/GaN HEMT, National Symposium on Compound Semiconductor Materials, Microwave Devices and Photoelectric Devices. 2008.

[11] Kong Xin, Wei Ke, Liu Guoguo, *et al*. Improvement of breakdown characteristics of an AlGaN/GaN HEMT with a U-type gate foot for millineter-Wave power application Chin. *Phys. B vol*. 21, No 12 (**2012**) 128501

[12] Zhang Y., Huang S., Wei K., *et al*. Millimeter-Wave AlGaN/GaN HEMTs With 43.6% Power-Added-Efficiency at 40 GHz Fabricated by Atomic Layer Etching Gate Recess [J]. *Ieee Electron Device Letters*, 2020, **41** (5): 701-704.

[13] S. Zhang, *et al*. "7.05 W/mm Power Density Millimeter-Wave GaN MIS-HEMT With Plasma Enhanced Atomic Layer Deposition SiN Dielectric Layer," in IEEE Electron Device Letters, vol. **42**, no. 10, pp. 1436-1439, Oct. 2021, doi: 10.1109/LED.2021.3105817.

[14] Shu Yang, Shenghou Liu, Yunyou Lu, *et al*. AC-Capacitance Techniques for Interface Trap Analysis in GaN-Based Buried-Channel MIS-HEMTs, IEEE TRANSACTIONS ON ELECTRON DEVICES, VOL. **62**, NO. 6, JUNE 2015, (pp. 1870-1878)